



**HAL**  
open science

# Steady-State Electrocatalytic Activity Evaluation with the Redox Competition Mode of Scanning Electrochemical Microscopy: A Gold Probe and a Boron-Doped Diamond Substrate

Olivier Henrotte, Alice Boudet, Ndrina Limani, Philippe Bergonzo, Bacem Zribi, Emmanuel Scorsone, Bruno Jusselme, Renaud Cornut

## ► To cite this version:

Olivier Henrotte, Alice Boudet, Ndrina Limani, Philippe Bergonzo, Bacem Zribi, et al.. Steady-State Electrocatalytic Activity Evaluation with the Redox Competition Mode of Scanning Electrochemical Microscopy: A Gold Probe and a Boron-Doped Diamond Substrate. *ChemElectroChem*, 2020, 7 (22), pp.4633-4640. 10.1002/celec.202001088 . cea-03014550

**HAL Id: cea-03014550**

**<https://cea.hal.science/cea-03014550>**

Submitted on 19 Nov 2020

**HAL** is a multi-disciplinary open access archive for the deposit and dissemination of scientific research documents, whether they are published or not. The documents may come from teaching and research institutions in France or abroad, or from public or private research centers.

L'archive ouverte pluridisciplinaire **HAL**, est destinée au dépôt et à la diffusion de documents scientifiques de niveau recherche, publiés ou non, émanant des établissements d'enseignement et de recherche français ou étrangers, des laboratoires publics ou privés.

1 Steady state electrocatalytic activity  
2 evaluation with the redox competition  
3 mode of SECM: the interests of a gold  
4 probe and a boron doped diamond  
5 substrate

6 Olivier Henrotte <sup>[a]</sup>, Alice Boudet <sup>[a]</sup>, Ndrina Limani <sup>[a]</sup>, Philippe Bergonzo <sup>[c]</sup>, Bacem Zribi <sup>[b]</sup>, Emmanuel  
7 Scorsone <sup>[b]</sup>, Bruno Joussetme <sup>[a]</sup> and Renaud Cornut <sup>[a]</sup>

8

9 [a] Dr. O. Henrotte, A. Boudet, N. Limani, Dr. B. Joussetme, Dr. R. Cornut  
10 Université Paris-Saclay, CEA, CNRS, NIMBE, LICSEN  
11 CEA Saclay 91191, Gif-sur-Yvette Cedex (France)

12

13 [b] Dr. B. Zribi, Dr. E. Scorsone  
14 Diamond Sensors Laboratory, LIST, CEA  
15 CEA Saclay 91191, Gif-sur-Yvette Cedex (France)

16

17 [c] Dr. P. Bergonzo  
18 Formerly [b], now at:  
19 Department of Electronic and Electrical Engineering, University College London  
20 17-19 Gordon Street, London, WC1H 0AH, United Kingdom

21

## 22 Abstract

23 In the current context of energetic transition, investigations of alternative complex systems require  
24 tools as scanning electrochemical microscopy (SECM) offering interesting opportunities as an  
25 electroanalytical technique to evaluate innovative catalysts. Herein, we demonstrate how a judicious  
26 choice of probe and substrate materials opens up improved performances to achieve steady state  
27 measurements for oxygen reduction reaction (ORR) catalytic activity detection through the redox  
28 competition scanning electrochemical microscopy (RC-SECM).

29 On the probe side, we show that using gold enhances the stability of the local oxygen concentration  
30 detection in comparison to the regularly used platinum one. On the substrate side, we evaluate boron  
31 doped diamond as an appealing alternative to classical support substrate, that shows a low ORR  
32 activity, high stability and very good reusability.

33 This work introduces an alternative approach for quantitative measurements with SECM, improving  
34 measurement easiness, comfort and reproducibility, thus paving the way towards standardized  
35 benchmarking and numerical simulation-based parameter extraction.

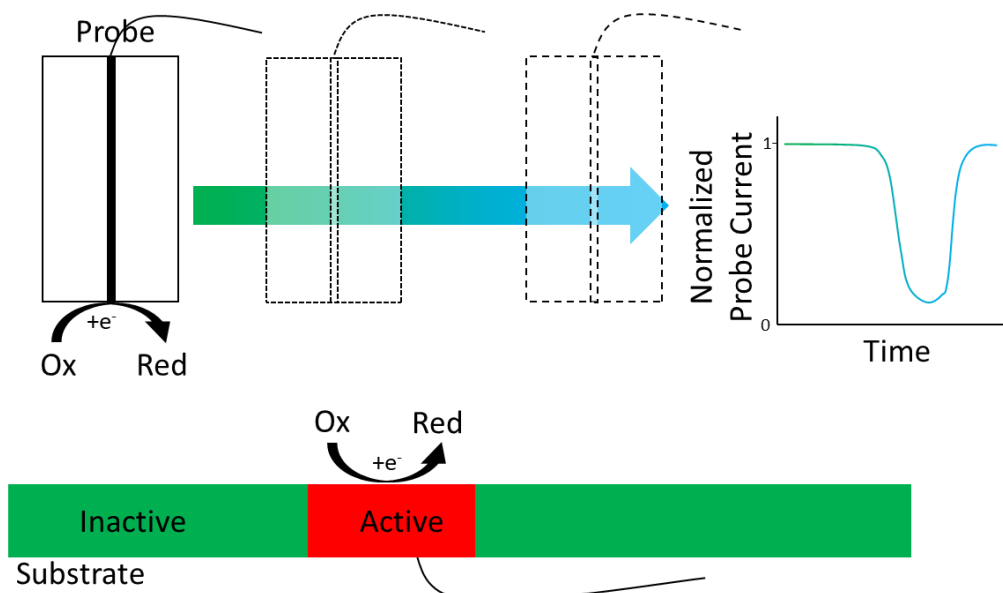
36

## 37 Introduction

38 The global energetic transition requires innovative tools enabling the evaluation of alternative  
39 materials and systems as candidates to perform energy. Fuel cells, and proton exchange membranes,  
40 for instance, are envisioned to play a key role as an efficient alternative technology. They are  
41 considered worldwide with high interests and could be easily adopted. However, the variety of  
42 catalysts presently under consideration by the community generates a high demand to enable their  
43 comparative characterization. Improved tools would help in their discrimination<sup>[1,2]</sup>. Presently  
44 characterization methods are the limiting part of innovation and improvements, particularly when  
45 active carbon based nanomaterials are concerned<sup>[3]</sup>. During the past decades, local probe techniques,  
46 such as scanning electrochemical microscopy (SECM) have made great progress. SECM already  
47 provides impressive results in the investigation of local electrochemical properties<sup>[4]</sup>. SECM is an  
48 electroanalytical tool that consists of a four-electrodes setup: two working electrodes (WE), namely a  
49 micrometric probe as an electrochemical sensor and a substrate to polarize the investigated material,  
50 a counter electrode (CE) and a reference electrode (RE). A potential can be applied on both the probe  
51 and the substrate while the probe is moved in the close vicinity of the substrate. The versatility of the  
52 technique allows it to be used in many different fields such as electrocatalysis<sup>[5,6]</sup>, corrosion<sup>[7]</sup>, photo-  
53 electrochemistry<sup>[8]</sup> or even DNA detection<sup>[9]</sup> or archaeological remains investigations<sup>[10]</sup>.

54 In the global research context of energetic transition, SECM has been used for the investigation of  
55 materials involved in energy related systems (batteries<sup>[11]</sup>, solar cells<sup>[12]</sup>, supercapacitors<sup>[13]</sup>, etc...), in  
56 particular for fuel cells (e.g. direct methanol fuel cell<sup>[14]</sup>, polymer electrolyte fuel cell<sup>[15]</sup>, proton  
57 exchange membrane fuel cell (PEMFC)<sup>[16-18]</sup>, etc...). The investigations here mainly focus on hydrogen  
58 evolution reaction (HER)<sup>[19]</sup> and more particularly on oxygen reduction reaction (ORR)<sup>[6,16,20]</sup> due to its  
59 slow kinetics, which constitutes a key point regarding the adoption of fuel cells at a large scale.

60 Regarding electrocatalytic activity assessment, the redox competition (RC) mode of SECM, introduced  
 61 by W. Schuhmann's group in 2006, is a recognised reference protocol<sup>[21]</sup>. It consists in polarizing the  
 62 probe and the substrate in such a way that the same reaction occurs on both sides: the probe then  
 63 evaluates the local reactant depletion due to its consumption by the electroactive sample (as shown  
 64 in Figure 1). A scan over the surface thus reveals the local activity variations.



65

66

Figure 1. Scheme of the RC-SECM mode.

67 RC mode has already been used to visualize the cell breathing<sup>[22]</sup>, to understand corrosion mechanism  
 68 on CrN film<sup>[23]</sup>, to study the consumption of oxygen from zinc oxide formation<sup>[24]</sup> or even to determine  
 69 more accurately enzymatic kinetics<sup>[25]</sup> thanks to previous modelling studies of such a system<sup>[26]</sup>. For  
 70 ORR catalysts, it operates in such a way that the scanning electrode is used as a probe of the local O<sub>2</sub>  
 71 concentration<sup>[18,21,27]</sup>. However, the use of the technique still remains mostly limited to the SECM  
 72 community, where studies are usually proof of concepts. We foresee that the expansion of the  
 73 technique to quantitative studies could provide better knowledge of many catalysts that are currently  
 74 being investigated within the context of the energetic transition. In fact SECM, and RC-SECM in  
 75 particular, are presently underused by the community, in comparison to the benefits the technique  
 76 can provide, namely its high resolution<sup>[28,29]</sup>.

77 The lack of a comfortable configuration that would enable better ease and reproducibility, and  
 78 particularly in complex conditions such as in acidic media to be compatible with PEMFC technology, is  
 79 a key obstacle to the development of the RC mode approach. Herein, we show how the choice of the  
 80 probe and substrate materials can help to stabilize the experimental configuration and enable steady  
 81 state measurements while scanning the surface.

82 Up to now, Pt microelectrodes are the most frequently used for the RC mode<sup>[18,21,27,30]</sup>, which is a  
83 rational choice considering the established electrocatalytic activity of this material towards ORR.  
84 However, Pt presents some drawbacks, for instance measurement instabilities are common at high  
85 probe current densities, and further it displays a high sensitivity to impurities that might be present in  
86 the solution. Subsequent alternatives such as the use of potential pulses<sup>[31]</sup> or high scan speeds<sup>[27]</sup> are  
87 required, but that may significantly hinder quantitative studies. On the other hand, gold as a probe  
88 metal has been used for other SECM measurements<sup>[16]</sup>, but –to the best of our knowledge– not for ORR  
89 detection. Here, we show that the low catalytic activity of gold is not an issue for ORR detection, which  
90 makes it suitable for studying ORR in RC mode, and even in acidic media.

91 In theory, the high sensitivity of the RC mode enables the evaluation of very low catalytic activities,  
92 however in this case, the substrate activity is likely to enter in competition with the catalytic  
93 material<sup>[32]</sup>. Overall ORR studies are usually performed using glassy carbon (GC) substrate<sup>[30,33,34]</sup>. Boron  
94 doped diamond (BDD) catalytic activity toward ORR has been investigated<sup>[35]</sup>, as other carbon based  
95 materials<sup>[36]</sup>. Furthermore, BDD has been used in SECM as a probe<sup>[37]</sup> or a studied material<sup>[35,38]</sup>, but  
96 not as substrate for ORR catalytic activity determination. BDD has shown higher overpotential for ORR,  
97 higher stability and lower H<sub>2</sub>O<sub>2</sub> production in acidic media compared to other carbon based  
98 substrates<sup>[39]</sup>. Here we demonstrate that BDD is an interesting alternative to standard carbon based  
99 substrates. We compared it to a GC substrate, due to its high representation in the literature, and a Si-  
100 wafer substrate covered with gold, as it is easy to produce, with good reproducibility and permits to  
101 achieve highly flat surface. The catalyst used to illustrate the potentiality of the new setup is a noble-  
102 metal free material based on carbon nanotubes (CNT) annealed with cobalt and nitrogen precursors<sup>[40]</sup>.

## 103 Experimental

### 104 Materials

105 All chemicals and solvents of research grade were purchased in the highest purity from Sigma Aldrich  
106 and used as received. All gases (nitrogen, oxygen) were of 99.995% purity. Commercial grade NC3100  
107 (purity >95%) multi-wall carbon nanotubes were obtained from Nanocyl (Belgium).

### 108 BDD substrate preparation

109 BDD was grown onto highly doped 4 inches silicon substrates by microwave plasma enhanced chemical  
110 vapor deposition (MPECVD) technique in a Seki Diamond AX6500 diamond growth reactor in a  
111 hydrogen plasma containing 1% methane as the source of carbon and trimethylboron as dopant. The  
112 resulting boron doping level is approximately  $2 \times 10^{21} \text{ cm}^{-3}$  as determined by secondary ion mass

113 spectrometry measurements. The polycrystalline diamond film obtained is approximately 1 micron  
114 thick.

### 115 BDD substrate cleaning process

116 BDD substrates were immersed into a piranha solution during 30 minutes and then in pure H<sub>2</sub>SO<sub>4</sub> at  
117 300°C for 30 minutes. Afterward, KNO<sub>3</sub> was added into the solution until a yellow coloration started to  
118 appear and the substrates stayed still 30 minutes more in the 300°C solution. Then, the substrates  
119 were rinsed into a 300°C pure H<sub>2</sub>SO<sub>4</sub> solution during 10 minutes and finally rinsed with distilled water.

120 In the case there was any doubt of catalyst residual traces on the substrate, a micro-wave hydrogen  
121 plasma exposure of the BDD surface, at a temperature of 600°C, was used to perform a complete  
122 reclaim of the BDD native surface.

### 123 Gold substrate preparation

124 Gold substrates were obtained by vacuum evaporation in a Balzers BAK 600 evaporator: a thin  
125 interlayer of chromium (to enhance gold adhesion on glass) and pure gold (99.99 % from Williams  
126 Advanced Materials) were evaporated at room temperature on silicium wafers. Prior to evaporation,  
127 the silicium wafers were rinsed 10 min under ultrasonication in water, ethanol and acetone  
128 successively. The thickness of the deposited layers was 3 nm of chromium and 30 nm of gold monitored  
129 in-situ by using a quartz crystal microbalance.

### 130 Catalyst preparation

131 The catalyst was prepared as described previously<sup>[40]</sup>. Briefly, Co(NO<sub>3</sub>)<sub>2</sub>·6H<sub>2</sub>O, multi-wall carbon  
132 nanotubes (MWNTs) and triazolopyridine (TAPy) were mixed in ethanol and sonicated for 30 minutes.  
133 Ethanol was removed under low pressure and the black Co-TAPy/CNTs powder was pyrolyzed at 950°C  
134 during 2h under argon. This catalyst will be called Co-N-NTC.

### 135 Catalyst deposition

136 The catalyst ink was prepared by dispersing Co-N-NTC powder (20 mg) with 5% in wt of D-520 Nafion  
137 in ethanol (1 mL) under sonication (30 min) with a cup-horn coupled with a Vibra-Cell (VCX 130 PB  
138 from Sonics Material). Afterwards, the total volume is increased with ethanol to 2 mL and the process  
139 is repeated. The same process continues by increasing the total volume to 5/10/20/50/100/200 mL to  
140 obtain a catalyst ink of 0.1 g.L<sup>-1</sup>.

141 The catalyst spot was obtained by two methods. The first one consists of dropping 2 mL of the catalytic  
142 ink onto the substrate heated at a temperature of 100°C with a micropipette. The second method uses  
143 the ExactaCoat apparatus from Sono-Tek to pulverize the solution onto the substrate. A mask with

144 micropatterns (from Micron Laser Technology) was used to obtain a controlled square spot in size and  
145 volume of solution deposited.

## 146 Instrumentation

### 147 AFM and SEM measurements

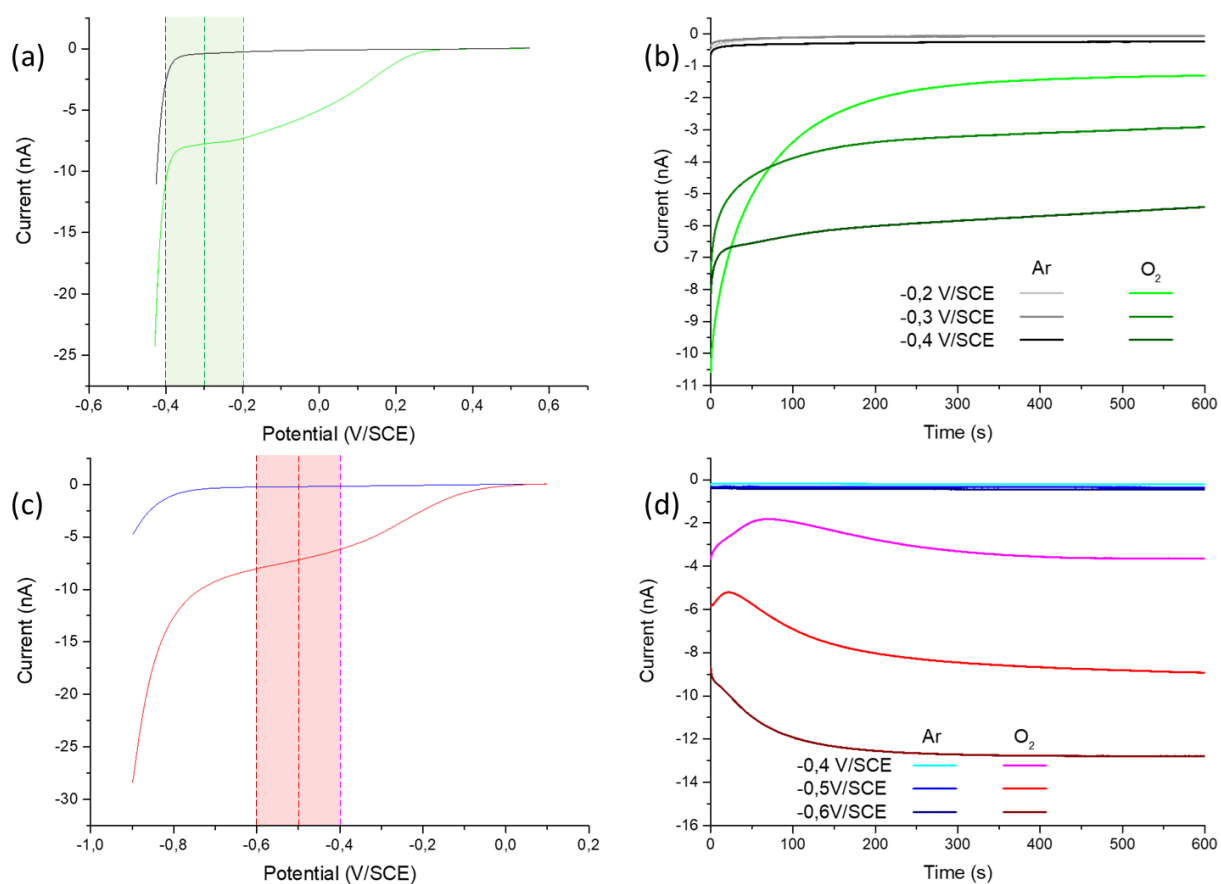
148 AFM images were performed on a Veeco Dimension 3100 equipped with a Nanoscope IIIa controller  
149 and analysed with the software Gwyddion. SEM images were recorded with a Hitachi S-4500 scanning  
150 electron microscope.

### 151 Electrochemical measurements

152 Electrochemical measurements were performed in sulfuric acid (Sigma Aldrich). The gold and platinum  
153 microelectrodes from Sensolytics had an active radius of 5 microns and a RG (the ratio between the  
154 inactive part radius and the active part radius of the probe) of 30. SECM experiments were performed  
155 on a modified M470 SECM Workstation from Bio-Logic Science Instruments. A four-electrode setup  
156 was used for the SECM experiments. It involved a platinum or a gold microdisk as first working  
157 electrode, a GC, a gold or a BDD substrate as second working electrode, a saturated calomel electrode  
158 (SCE) as reference and a net made of platinum wires as counter electrode. Both reference and counter  
159 electrodes are placed in sintered guards to avoid direct contact between the analysed solution, the  
160 reference and the counter electrodes. The probe-substrate distance was evaluated by approaching the  
161 probe in the vicinity of the area of interest, somewhere without catalyst, and by letting the substrate  
162 at open circuit potential (OCP). In this case a negative feedback was obtained, and a comparison with  
163 theory provides the relationship between the probe position and the probe-substrate distance<sup>[41,42]</sup>.  
164 Unless mentioned, the analysis of the ORR activity was made in H<sub>2</sub>SO<sub>4</sub> 0.1 M solution. The probe was  
165 stabilized 300 s before each measurement.

## 166 Results & discussion

167 The working electrodes are central to the SECM technique. Improving both of them to specific  
168 demands allows progresses in the quality of measurements. First, in order to investigate the first  
169 working electrode, i.e. the probe, a linear sweep voltammetry (LSV) is performed from OCP up to the  
170 solvent reduction signal, in Ar saturated solution and O<sub>2</sub> saturated solution. At this step, the probe is  
171 put in solution without the substrate to avoid any interaction.



172

173 *Figure 2. (a) LSV at the platinum probe from 0.55 to -0.43 V/SCE with a 10 mV/s scan rate. (b) CA at the platinum probe at*  
 174 *different potentials (-0.2, -0.3 and -0.4 V/SCE). Black curves for Ar saturated solution and green curves for O<sub>2</sub> saturated solution*  
 175 *in (a & b). (c) LSV at the gold probe from 0.1 to -0.9 V/SCE with a 10 mV/s scan rate. (d) CA at the gold probe at different*  
 176 *potentials (-0.4, -0.5 and -0.6 V/SCE). Blue curves for Ar saturated solution and red curves for O<sub>2</sub> saturated solution in (c & d).*  
 177 *All measurements were made in H<sub>2</sub>SO<sub>4</sub> 0.1M, r<sub>T</sub> = 5 μm and RG = 30 for both probes.*

178 As shown in Figure 2.a, a well-defined plateau is observed between -0.2 to -0.4 V/SCE for the ORR at  
 179 the platinum probe, illustrated by the green bar. Several potentials of this plateau are then tested by  
 180 chronoamperometry (CA). Each potential is applied for 600 seconds, in order to investigate the stability  
 181 of the measurement. The probe is polished and cleaned between each measurement and the  
 182 procedure is repeated several times in the O<sub>2</sub> saturated solution. The results presented Figure 2.b show  
 183 the currents measured at -0.2, -0.3 and -0.4 V/SCE. For the three potentials, an exponential loss of  
 184 current is observed, followed by a stabilization of the slope to a non 0 value. This behaviour is not the  
 185 one expected from a well-defined diffusion plateau as observed on the CV. Furthermore, the current  
 186 variation during the first 200 seconds is not exclusively due to the establishment of the diffusion profile  
 187 in the vicinity of the probe, as this is a process that has time constant of typically seconds<sup>[43]</sup>. It is also  
 188 related to the evolution of platinum surface states, with possibly some contamination due to side  
 189 reactions. Furthermore, the current densities are not the same along the probe surface increasing the  
 190 complexity of such phenomenon. In any case, the observation is in accordance with what is observed

191 in the literature<sup>[21]</sup>. In any case, the important element for SECM imaging is to have a steady-state  
 192 current at the probe. The Pt probe current was the most stabilized after 300s with a linear loss of  
 193 current. After this stabilization step, the sensitivity, the detection threshold and the instability can be  
 194 then evaluated. These values are shown in Table 1. We evaluated the theoretical sensitivity by using  
 195 the equation of the current at a diffusion plateau<sup>[44]</sup>. In the equation 1, n is the number of electrons  
 196 exchanged (4 in the case of a complete O<sub>2</sub> reduction), F is the Faraday constant, D<sub>0</sub> is the diffusion  
 197 coefficient of O<sub>2</sub> in H<sub>2</sub>SO<sub>4</sub> (1.4x10<sup>-5</sup> cm<sup>2</sup>.s<sup>-1</sup> for 0.5M)<sup>[45]</sup>, C<sub>0</sub> is the concentration of O<sub>2</sub> in H<sub>2</sub>SO<sub>4</sub> (in the  
 198 case of an O<sub>2</sub> saturated H<sub>2</sub>SO<sub>4</sub> 0.1M solution, it is 1.27x10<sup>-6</sup> mol.cm<sup>-3</sup> at 298K)<sup>[46]</sup> and r<sub>T</sub> is the radius of  
 199 the active part of the electrode. The theoretical sensitivity is 10.8 nA/mM(O<sub>2</sub>). The sensitivity measured  
 200 at t<sub>600</sub> is 1.0, 2.2 and 4.3 nA/mM(O<sub>2</sub>) for -0.2, -0.3 and -0.4 V/SCE respectively, which are significantly  
 201 lower values compared to the theoretical one. It can be noticed that the sensitivity measured at t<sub>0</sub> is  
 202 8.3, 5.9 and 6.4 respectively which is closer to the theoretical one.

$$203 \quad I = 4nFD_0C_0r_T \quad (1)$$

204 We decided to consider the detection threshold as the O<sub>2</sub> concentration for a current equal to the  
 205 current measured in absence of O<sub>2</sub> in solution. This is calculated by the equation 2 where I<sub>O<sub>2</sub></sub> is the  
 206 current measured in the O<sub>2</sub> saturated solution and I<sub>Ar</sub>, the current measured in the Ar saturated  
 207 solution. For -0.2, -0.3 and -0.4 V/SCE, the detection threshold is 47, 31 and 46 μM(O<sub>2</sub>) respectively.

$$208 \quad \text{Detection threshold} = \frac{C_0}{I_{O_2} \times I_{Ar}^{-1}} \quad (2)$$

209 Besides, the instability of the measurement is evaluated by considering the current difference between  
 210 480 and 600 s to have a well-defined slope compared to 300 s where the stabilization occurs (see  
 211 equation 3, where I<sub>600</sub> is the current at t<sub>600</sub>, I<sub>480</sub> is the current at t<sub>480</sub> and I<sub>m</sub> is the averaged current  
 212 between t<sub>480</sub> and t<sub>600</sub>).

$$213 \quad \text{Instability} = \left| \frac{I_{600} - I_{480}}{t_{600} - t_{480}} \times \frac{1}{I_m} \right| \times 100 \quad (3)$$

214 The calculated instability is expressed in %/min which corresponds to the current percentage loss every  
 215 minute of the measurement. In the case of the Pt probe, the instability is 0.44, 0.62 and 0.44 for -0.2,  
 216 -0.3 and -0.4 V/SCE respectively.

217 Exactly the same procedure is applied to the gold probe. The LSV and the CA are presented in Figure  
 218 2.c and Figure 2.d respectively. In this case, a pseudo-plateau between -0.4 to -0.7 V/SCE is observed  
 219 (illustrated by the red bar) in the ORR window instead of a well-defined diffusion plateau. Different CA  
 220 were done in the same condition as previously for the platinum probe, except that the chosen  
 221 potentials are -0.4, -0.5 and -0.6 V/SCE, in accordance with the observed lower electrocatalytic activity

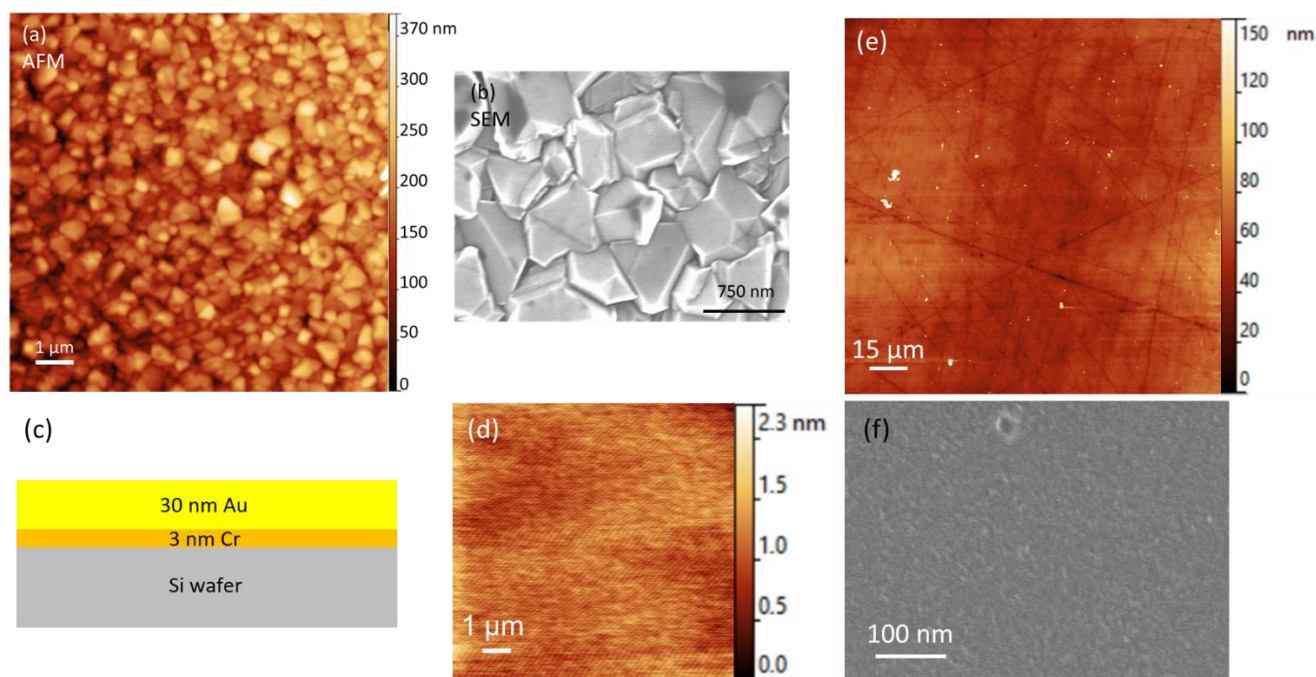
222 of gold versus platinum. Here also, stabilisation of measurements lasted about 300 s. The shape of the  
 223 current curves is different in the case of gold. Here again, the probe's surface state impacts positively  
 224 or negatively the kinetics at the surface. The difference between Pt and Au probes can be explained by  
 225 their different ORR mechanisms occurring at the surface, as well as the difference in the stability of the  
 226 surface states. It can be noticed in the Figure 2.d that the stabilized current is close to the starting  
 227 current. Thus, for the gold probe, the sensitivity calculated is 3.3, 7.4 and 10.0 nA/mM(O<sub>2</sub>) for -0.4, -  
 228 0.5 and -0.6 V/SCE respectively. The detection threshold is 63, 49 and 46 μM(O<sub>2</sub>) and the instability is  
 229 0.62, 0.13 and 0.19 %/min respectively. The sensitivity at -0.6 V/SCE is close to the theoretical one. As  
 230 an additional advantage, the use of a gold probe permits to avoid the possibility to contaminate the  
 231 substrate with a highly active material such as platinum. Moreover, the stability of the current at the  
 232 gold probe allows long time acquisition with steady-state measurements. Therefore, based on the  
 233 comparison of their sensitivities, their detection thresholds and their instabilities between platinum  
 234 and gold probes, the latter really appears as a very interesting alternative probe for studying ORR.

235 *Table 1. Averaged values from the CA at the probes at t<sub>600s</sub> and calculated sensitivity, detection threshold and instability for*  
 236 *these values.*

| Active part composition | E <sub>probe</sub> (V/SCE) | Current at t <sub>600s</sub> (nA) Ar <sub>sat</sub> | Current at t <sub>600s</sub> (nA) O <sub>2</sub> sat | Sensitivity (nA/mM(O <sub>2</sub> )) | Detection threshold (μM(O <sub>2</sub> )) | Instability (%/min) |
|-------------------------|----------------------------|-----------------------------------------------------|------------------------------------------------------|--------------------------------------|-------------------------------------------|---------------------|
| <b>Platinum probe</b>   | -0.2                       | -0.04                                               | -1.22                                                | 1.0                                  | 46                                        | 0.44                |
|                         | -0.3                       | -0.07                                               | -2.83                                                | 2.2                                  | 31                                        | 0.62                |
|                         | -0.4                       | -0.20                                               | -5.48                                                | 4.3                                  | 46                                        | 0.44                |
| <b>Gold probe</b>       | -0.4                       | -0.21                                               | -4.27                                                | 3.3                                  | 63                                        | 0.62                |
|                         | -0.5                       | -0.36                                               | -9.39                                                | 7.4                                  | 49                                        | 0.13                |
|                         | -0.6                       | -0.46                                               | -12.72                                               | 10.0                                 | 46                                        | 0.19                |

237

238 The supporting substrate used to analyse the activity of a catalyst is another important element for  
 239 electrochemical measurements. Micrometric planarity, roughness and electrochemical activity are key  
 240 parameters that influence the analysis. Figure 3 shows AFM (a) and SEM (b) images of a BDD substrate,  
 241 where one can observe its polycrystallinity. The roughness average (Ra) and the root-mean-square  
 242 roughness (Rq) of BDD is measured by AFM and is 39.9 nm and 50.0 nm respectively. Moreover, the  
 243 maximum measured height is 372 nm. In the present work, a micrometric probe is used, and the  
 244 positioning is performed at the micrometric scale (typically 30 microns, as shown Figure 5), so the ~100  
 245 nm roughness of the sample is negligible<sup>[49]</sup>. Besides, the use of a Si-wafer as substrate support  
 246 guaranties a negligible non-planarity of the whole sample. Thus, the topography of the BDD substrate  
 247 is highly acceptable for the investigation of micrometric spots of catalysts with the RC-mode and a  
 248 micrometric probe.

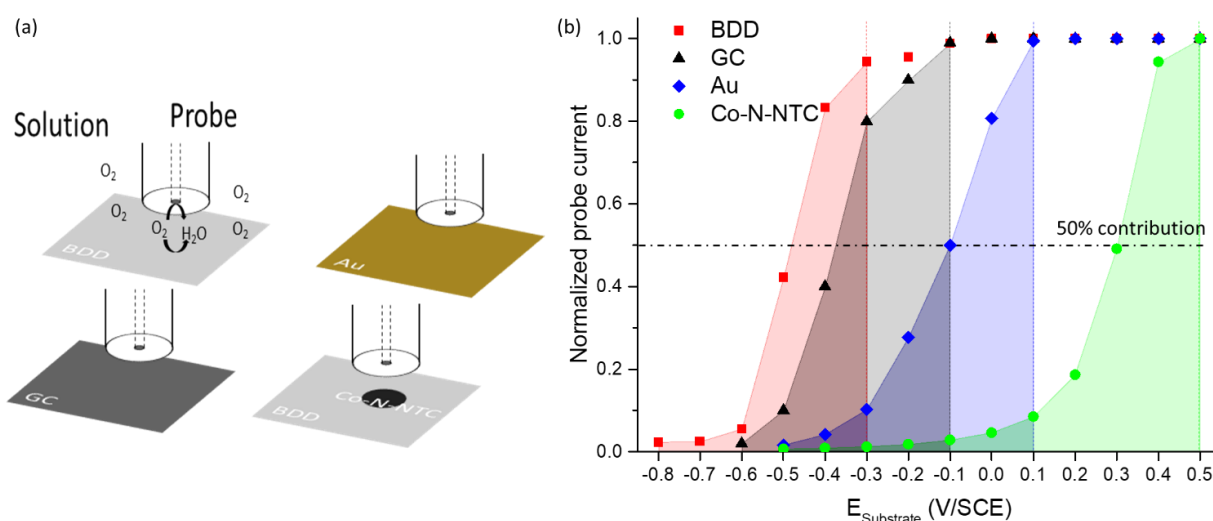


249

250 *Figure 3. (a) AFM image showing a thickness of 372 nm, Ra of 39.9 nm and Rq of 50.0 nm and (b) SEM image showing crystals*  
 251 *smaller than 1 μm in diameter of a BDD substrate. (c) Scheme of the gold substrate structure. (d) AFM image showing a 2.3*  
 252 *nm thickness, Ra of 178 pm and Rq of 225 pm of a gold substrate. (e) AFM image showing a GC substrate with a Ra of 7.2 nm*  
 253 *and a Rq of 11.4 nm. (f) SEM image of a GC substrate.*

254 As an alternative to BDD, a Si-wafer covered with gold and a GC substrate can be considered. The gold  
 255 substrate structure is illustrated in Figure 3.c and d for the AFM image. The maximum measured height  
 256 is 2.3 nm with a Ra of 178 pm and a Rq of 225 pm which allows to scan on a nanoscale surface where  
 257 inhomogeneities come from the investigated material only. The AFM and SEM image of a GC substrate  
 258 are presented in Figure 3.e and f respectively. The maximum height measured on the GC substrate is  
 259 almost 650 nm despite a Ra of 7.2 nm and a Rq of 11.4 nm. The average value is 58.3 nm meaning  
 260 there is scarce but important inhomogeneities on the GC substrate. The polishing process of the GC  
 261 substrate is of the outmost importance to allows a high planarity and so nanoscale measurements on  
 262 it. In contrary, gold and BDD substrates, thanks to the Si-wafer support, keep their planarity on the  
 263 whole surface.

264 Electrochemical results are presented Figure 4 comparing BDD to a GC substrate, a gold substrate and  
 265 a catalyst spot of Co-N-NTC deposited on BDD. The samples are studied by RC-SECM at a constant  
 266 height with a probe-substrate distance of 50 μm. The process involved is presented Figure 4.A and is  
 267 done in acidic media saturated with oxygen (H<sub>2</sub>SO<sub>4</sub> 0.1 M) due to the acidic condition used in a PEMFC.



268

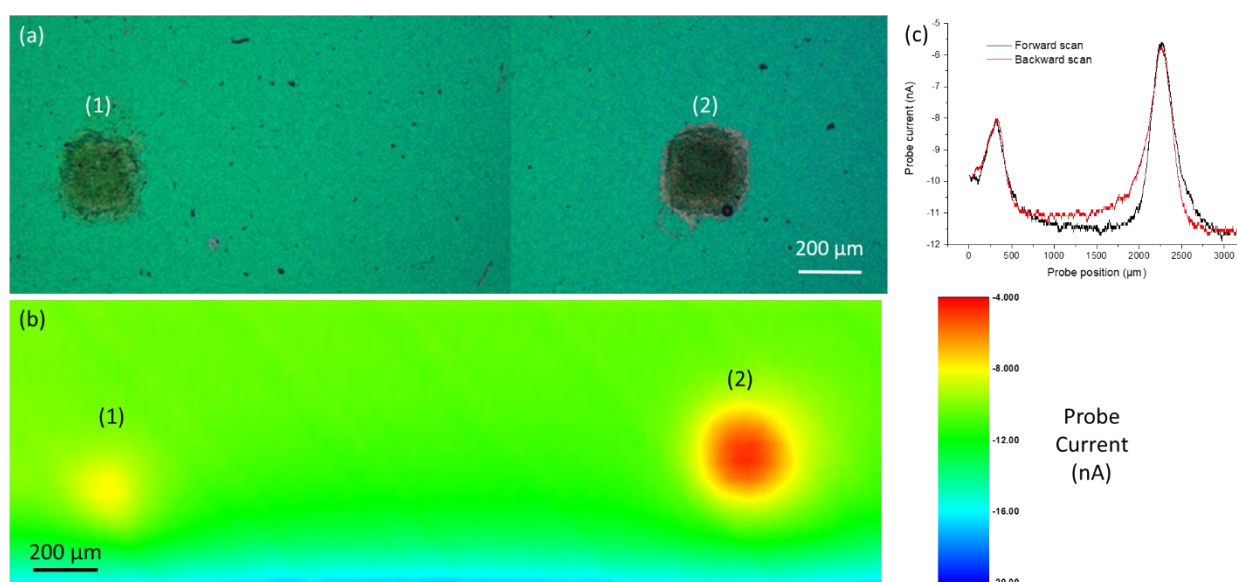
269 Figure 4. (a) Scheme presenting the process involved in the RC-SECM measurement to analyse the ORR activity of BDD, GC, Au  
 270 and the catalyst spot. (b) Results of chronoamperometry (CA) at different substrate potentials with a gold probe ( $r_T = 5 \mu\text{m}$ ,  
 271  $RG = 30$ ,  $E_{\text{probe}} = -0.6\text{V/SCE}$ ) in  $\text{H}_2\text{SO}_4$  0.1 M solution saturated with oxygen and with a distance probe-substrate of  $50 \mu\text{m}$ .  
 272 Measurements are made on a clean BDD substrate (■), a clean GC substrate (▲), a clean gold substrate (◆) and a Co-N-NTC  
 273 spot (●). The area under the curves represent the potential zone where the competition between the probe and the substrate  
 274 occurs.

275 The probe was held at  $-0.6 \text{ V/SCE}$  in order to reduce  $\text{O}_2$  during all measurements. Samples were held  
 276 at different potentials, from one from which the sample is inactive, to one corresponding to a high  
 277 activity of the sample (almost no current at the probe) with a  $100 \text{ mV}$  difference between each  
 278 measurement. Each potential was held at least  $100 \text{ s}$  for the current to reach a plateau once stabilized.  
 279 The results of the experiment are presented in Figure 4.b.

280 The competition starting point between the probe and the samples is noticed at a potential between  
 281  $0.5$  and  $0.4 \text{ V/SCE}$  for the Co-N-NTC spot,  $0.1 \text{ V/SCE}$  for the gold substrate, between  $-0.1$  and  $-0.2 \text{ V/SCE}$   
 282 for the GC substrate and  $-0.3 \text{ V/SCE}$  for the BDD substrate. This means that the competition occurs for  
 283 more negative potentials applied to the substrate than the one of this starting point. A  $50 \%$   
 284 contribution of samples is observed at  $0.3 \text{ V/SCE}$  for the Co-N-NTC spot,  $-0.1 \text{ V/SCE}$  for the gold  
 285 substrate,  $-0.41 \text{ V/SCE}$  for the GC substrate and  $-0.48 \text{ V/SCE}$  for the BDD substrate. Finally, the probe  
 286 measures a current almost null at  $-0.2 \text{ V/SCE}$  for the Co-N-NTC spot,  $-0.5 \text{ V/SCE}$  for the gold substrate  
 287 and  $-0.7 \text{ V/SCE}$  for the BDD. However, for the GC substrate, even at the lowest potentials, the probe  
 288 current was not null. This can be explained by an incomplete ORR at the GC substrate. These results  
 289 showed that the BDD substrate is less active than the other substrates. Moreover, according to  
 290 previous investigations made for GC through cyclic voltammetry, the same conclusion was established  
 291 in acidic<sup>[39]</sup> and alkaline media<sup>[50]</sup>.

292 Overall, the large inactive window of BDD -until -0.3 V/SCE no contribution from the substrate is  
293 observed- offers a wider range of experimental conditions that can be used, as illustrated with the Co-  
294 N-NTC spot with a loading around  $200 \mu\text{g}/\text{cm}^2$ . There, the  $\text{O}_2$  consumption by the catalyst is total before  
295 the  $\text{O}_2$  consumption starts at the substrate, which is not the case with gold. This proves that much  
296 lower electrocatalytic activities or loadings can be investigated with BDD.

297 In order to further show that gold probe and BDD substrate are suitable to perform SECM imaging at  
298 steady state, Figure 5.a shows a  $3 \text{ mm}^2$  optical image of two Co-N-NTC spots of 120 (a) and 230 (b)  
299  $\mu\text{g}/\text{cm}^2$  sprayed with the ExactaCoat system through a micro-patterned mask to obtain this well-  
300 defined square spots. The RC-SECM image of these spots is shown in Figure 5.b at  $E_{\text{substrate}} = -0.3 \text{ V/SCE}$ .  
301 The full RC-SECM image (with both forward and backward scans) is recorded within 2 hours.



302  
303 *Figure 5. (a) Optical image of (1)  $120 \mu\text{g}/\text{cm}^2$  and (2)  $230 \mu\text{g}/\text{cm}^2$  Co-N-NTC spots on a BDD substrate. (b) RC-SECM image of  
304 the spots shown in (a). (c) RC-SECM forward (black curve) and backward (red curve) linescans at  $Y = 450 \mu\text{m}$  from the RC-SECM  
305 image (b) corresponding. SECM experiments done with a gold probe ( $r_T = 12 \mu\text{m}$ ,  $RG = 11$ ,  $E_{\text{probe}} = -0.45 \text{ V/SCE}$ ) in  $\text{H}_2\text{SO}_4$  0.1 M  
306 solution saturated with oxygen and with  $E_{\text{substrate}} = -0.3 \text{ V/SCE}$ , a distance probe-substrate of  $30 \mu\text{m}$  and  $v_{\text{scan}} = 20 \mu\text{m}/\text{s}$ .*

307 As shown in Figure 5.c, forward and backward linescans overlap above the active spot, and this proves  
308 the steady state nature of the measurement. Still, non-stationarity can be seen when the probe is at  
309 the extremity of the spots, and in this case the current is smaller if the probe is approaching the center  
310 of the spot, and larger in the contrary. This fits the expectations, and does not affect the maximal  
311 current variation, which is the most important parameter regarding the spot electrocatalytic activity  
312 evaluation. At each line of the image, the current obtained far from the spots can be used to calibrate  
313 the relationship between the measured current and the oxygen concentration, by evaluating the  
314 effective number of electrons transferred:

315 
$$n = \frac{I}{4FD_0C_0r_T\beta(RG)NiT(L, RG)} \quad (4)$$

316 with  $\beta(RG)$ , a correction factor due to the enhancement of diffusion limiting current for the small RG  
317 values<sup>[51]</sup> and  $NiT(L, RG)$ , a correction factor due to diffusion hindering similar than a negative  
318 feedback<sup>[42]</sup>. With the experimental conditions of Figure 5.c (RG = 11, L = 2.5; L being the ratio between  
319 the distance probe-substrate with the  $r_T$ ),  $NiT(L, RG) = 0.79$  so  $n = 1.8$  with the current measured at  
320 the end of the linescan (-11.5 nA) presented Figure 5.c. Alternatively,  $NiT(L, RG) = 0.78$  is the ratio  
321 between the current measured far from the spot, divided by the current measured in solution.  $n$  is  
322 smaller than 2 here probably because the diffusion plateau is not reached at the working potential.

323 This way, the quantification of the oxygen consumption rate will become possible. It will need the  
324 support of numerical simulation, explicitly taking into account the experimental parameters such as  
325 the probe-to-substrate distance, the probe size (active and inactive part), and the spot size and shape.  
326 This is fully justified in a context of performing the benchmarking of catalysts, which will be done in  
327 future works.

## 328 Conclusion

329 Herein, we showed how steady state evaluation by RC-SECM for ORR detection in acidic conditions can  
330 be achieved with gold probes and BDD substrates. The gold probe exhibited a remarkable current  
331 stability, with variation values under 0.2 % variation per minute), further to a good sensitivity and a  
332 detection threshold similar to that of the platinum probe. Similarly, we also demonstrated that BDD as  
333 supporting substrate shows a very large inactivity window, up to -0.3 V vs SCE, with a submicrometric  
334 roughness and a small long-distance non-planarity, thanks to the Si-wafer support underneath. The  
335 same setup can also be considered for alkaline media investigations. This may be the basis of future  
336 works. Furthermore, preparation of flat BDD substrates is also planned in the future.

## 337 Conflicts of interest

338 The authors have no conflict of interest to declare.

## 339 Acknowledgement

340 The authors acknowledge the SENTINEL project, funded by the European Union's Horizon 2020  
341 research and innovation program under the Marie Skłodowska-Curie grant agreement no 812398, and  
342 the PEGASUS project, funded by the European Union's Horizon 2020 research and innovation program  
343 FCH-01-2-2017, no779550.

344

345

346

## 347 References

- 348 [1] J. Heinze, *Angew. Chemie Int. Ed. English*, **1993**, 32, 1268–1288.
- 349 [2] A. Dobrzeniecka *et al.*, *Catal. Today*, **2013**, 202, 55–62.
- 350 [3] A. S. Arico, P. Bruce, B. Scrosati, J. M. Tarascon, and W. Van Schalkwijk, *Nat. Mater.*, **2005**, 4,  
351 366–377.
- 352 [4] Y. Yu, T. Sun, and M. V. Mirkin, *Anal. Chem.*, **2015**, 87, 7446–7453.
- 353 [5] C. M. Sánchez-Sánchez, J. Rodríguez-López, and A. J. Bard, *Anal. Chem.*, **2008**, 80, 3254–3260.
- 354 [6] A. Minguzzi, M. A. Alpuche-Aviles, J. R. Lopez, S. Rondinini, and A. J. Bard, *Anal. Chem.*, **2008**,  
355 80, 4055–4064.
- 356 [7] J. J. Santana, J. Gonzalez-Guzman, L. Fernandez-Merida, S. Gonzalez, and R. M. Souto,  
357 *Electrochim. Acta*, **2010**, 55, 4488–4494.
- 358 [8] J. Y. Kim, H. S. Ahn, and A. J. Bard, *Anal. Chem.*, **2018**, 90, 3045–3049.
- 359 [9] A. Domenech-Carbo *et al.*, *Electrochim. Acta*, **2014**, 115, 546–552.
- 360 [10] A. Domenech-Carbo, M. Teresa Domenech-Carbo, M. Lastras Perez, and M. Herrero-Cortell,  
361 *Forensic Sci. Int.*, **2015**, 247, 79–88.
- 362 [11] J. Hui, M. Burgess, J. Zhang, and J. Rodriguez-Lopez, *ACS Nano*, **2016**, 10, 4248–4257.
- 363 [12] K. C. Huang *et al.*, *J. Mater. Chem.*, **2011**, 21, 10384–10389.
- 364 [13] A. Sumboja, U. M. Tefashe, G. Wittstock, and P. S. Lee, *J. Power Sources*, **2012**, 207, 205–211.
- 365 [14] Z. Wang, Y. Liu, and V. M. Linkov, *J. Power Sources*, **2006**, 160, 326–333.
- 366 [15] A. Kishi, M. Inoue, and M. Umeda, *J. Phys. Chem. C*, **2010**, 114, 1110–1116.
- 367 [16] J. L. Fernández, D. A. Walsh, and A. J. Bard, *J. Am. Chem. Soc.*, **2005**, 127, 357–365.
- 368 [17] W. Li, F.-R. F. Fan, and A. J. Bard, *J. Solid State Electrochem.*, **2012**, 16, 2563–2568.
- 369 [18] S. Kundu *et al.*, *J. Phys. Chem. C*, **2009**, 113, 14302–14310.
- 370 [19] S. Kumar, P. K. Sahoo, and A. K. Satpati, *ACS Omega*, **2017**, 2, 7532–7545.
- 371 [20] G. J. Lu, J. S. Cooper, and P. J. McGinn, *Electrochim. Acta*, **2007**, 52, 5172–5181.
- 372 [21] K. Eckhard, X. Chen, F. Turcu, and W. Schuhmann, *Phys. Chem. Chem. Phys.*, **2006**, 8, 5359–

- 373 5365.
- 374 [22] M. Nebel, S. Grützke, N. Diab, A. Schulte, and W. Schuhmann, *Faraday Discuss.*, **2013**, 164, 19–  
375 32.
- 376 [23] S. Gao, C. Dong, H. Luo, K. Xiao, X. Pan, and X. Li, *Electrochim. Acta*, **2013**, 114, 233–241.
- 377 [24] S. Thomas *et al.*, *J. Appl. Electrochem.*, **2014**, 44, 747–757.
- 378 [25] I. Morkvenaite-Vilkonciene, A. Ramanaviciene, P. Genys, and A. Ramanavicius, *Electroanalysis*,  
379 **2017**, 29, 1532–1542.
- 380 [26] F. Ivanauskas, I. Morkvenaite-Vilkonciene, R. Astrauskas, and A. Ramanavicius, *Electrochim.*  
381 *Acta*, **2016**, 222, 347–354.
- 382 [27] A. J. Wain, *Electrochim. Acta*, **2013**, 92, 383–391.
- 383 [28] P. Sun and M. V. Mirkin, *Anal. Chem.*, **2006**, 78, 6526–6534.
- 384 [29] B. B. Katemann, A. Schulte, and W. Schuhmann, *Electroanalysis*, **2004**, 16, 60–65.
- 385 [30] A. Tiwari, V. Singh, D. Mandal, and T. C. Nagaiah, *J. Mater. Chem. A*, **2017**, 5, 20014–20023.
- 386 [31] X. X. Chen, A. J. R. Botz, J. Masa, and W. Schuhmann, *J. Solid State Electrochem.*, **2016**, 20, 1019–  
387 1027.
- 388 [32] T. Löffler, P. Wilde, D. Öhl, Y. T. Chen, K. Tschulik, and W. Schuhmann, *Faraday Discuss.*, **2018**,  
389 210, 317–332.
- 390 [33] B. Lim *et al.*, *Science (80-. )*, **2009**, 324, 1302–1305.
- 391 [34] L. Qu, Y. Liu, J. Baek, and L. Dai, *ACS Nano*, **2010**, 4, 1321–1326.
- 392 [35] V. S. Dilimon, N. S. V. Narayanan, and S. Sampath, *Electrochim. Acta*, **2010**, 55, 5930–5937.
- 393 [36] G. Wu and P. Zelenay, *Acc. Chem. Res.*, **2013**, 46, 1878–1889.
- 394 [37] K. B. Holt, J. Hu, and J. S. Foord, *Anal. Chem.*, **2007**, 79, 2556–2561.
- 395 [38] S. Tan *et al.*, *Phys. Chem. Chem. Phys.*, **2017**, 19, 8726–8734.
- 396 [39] M. Gara and R. G. Compton, *New J. Chem.*, **2011**, 35, 2647–2652.
- 397 [40] A. Morozan, P. Jégou, B. Josselme, and S. Palacin, *Phys. Chem. Chem. Phys.*, **2011**, 13, 21600–  
398 21607.
- 399 [41] B. R. Horrocks, M. V. Mirkin, and A. J. Bard, *J. Phys. Chem.*, **1994**, 98, 9106–9114.

- 400 [42] R. Cornut and C. Lefrou, *J. Electroanal. Chem.*, **2007**, 608, 59–66.
- 401 [43] M. V. Mirkin and S. Amemiya, *Nanoelectrochemistry*, in *CRC Press*, CRC Press, 2015, 439–461.
- 402 [44] K. Aoki and J. Osteryoung, *J. Electroanal. Chem. Interfacial Electrochem.*, **1981**, 122, 19–35.
- 403 [45] J. J. Salvador-Pascual, S. Citalán-Cigarroa, and O. Solorza-Feria, *J. Power Sources*, **2007**, 172,  
404 229–234.
- 405 [46] T. N. Das, *Ind. Eng. Chem. Res.*, **2005**, 44, 1660–1664.
- 406 [47] Y. Shen, M. Trauble, and G. Wittstock, *Anal. Chem.*, **2008**, 80, 750–759.
- 407 [48] A. M. Gómez-Marín, A. Boronat, and J. M. Feliu, *Russ. J. Electrochem.*, **2017**, 53, 1029–1041.
- 408 [49] F. O. Laforge, J. Velmurugan, Y. Wang, and M. V Mirkin, *Anal. Chem.*, **2009**, 81, 3143–3150.
- 409 [50] T. Yano, D. A. Tryk, K. Hashimoto, and A. Fujishima, *J. Electrochem. Soc.*, **1998**, 145, 1870–1876.
- 410 [51] C. Lefrou and R. Cornut, *ChemPhysChem*, **2010**, 11, 547–556.

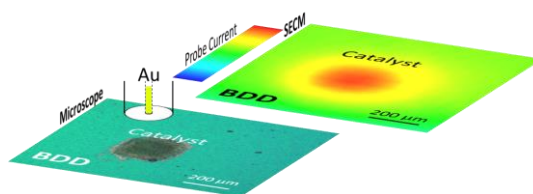
411

412

# Table of Contents

413

414



415

416 This paper demonstrates how a judicious choice of probe and substrate materials opens up improved  
417 performances to achieve steady state measurements, in this case, for oxygen reduction reaction (ORR)  
418 catalytic activity detection through the redox competition scanning electrochemical microscopy (RC-  
419 SECM).

420 We show that the use of gold enhances the stability of the local oxygen concentration detection in  
421 comparison to the regularly used platinum one. We evaluate boron doped diamond as an appealing  
422 support substrate, that shows a low ORR activity, high stability and very good reusability.

423

424

## 425 Keywords

426 Boron doped diamond; Electrocatalysis; ORR; Redox competition mode; SECM

427